Analogous Hawking radiation from gapped excitations in a transonic flow of binary Bose-Einstein condensates

Wei-Can Syu* and Da-Shin Lee†

Department of Physics, National Dong-Hwa University, Hualien 974301, Taiwan, Republic of China

(Received 13 December 2022; accepted 4 April 2023; published 28 April 2023)

We have studied analytically the approximate solutions to the gapped mode equations in the hydrodynamic regime for a class of binary Bose-Einstein condensate acoustic black holes. The horizon from the transonic flow is formed by manipulating the phonon sound speed and the flow velocity with the experimentally accessible parameters. The asymptotic modes of various scattering processes are constructed from which to obtain scattering coefficients and then to further decompose the field operator in terms of the asymptotic states. Also, the Unruh state is introduced to be the appropriate state for the description of gravitational collapse of the black hole. The particle densities of the outgoing modes are computed. The effective energy gap term in the dispersion relation of the gapped excitations introduces the threshold frequency ω_r in the subsonic regime, below which the propagating modes do not exist. Thus, the particle spectrum of the analogous Hawking modes in the exterior of the horizon of the subsonic region significantly deviates from that of the gapless cases near the threshold frequency due to the modified graybody factor, which vanishes as the mode frequency is below ω_r. However, in the interior region of the horizon of the supersonic region, the spectrum of the particle production of the Hawking partner has the nonthermal feature. The correlators between the analog Hawking mode and its partner of relevance to the experimental observations are also investigated and show some peaks near the threshold frequency ω_r resulting from the gap energy term to be seen in future experiments.

DOI: 10.1103/PhysRevD.107.084049

I. INTRODUCTION

The evaporation of black holes has been predicted by Hawking through the emission of a thermal flux of radiation, thereby reducing its mass [1]. However, the expected Hawking temperature is of order of $T_H = 6.0 \times 10^{-8}$ K for an astrophysical black hole, which is several orders of magnitude smaller than the cosmic microwave background temperature $T_{\rm cmb} \approx 3$ K. Thus, the detection of Hawking radiation in an astrophysical context is extremely unlikely. The program of the analog models of gravity due to the pioneering work of Unruh is an attempt to implement laboratory systems to mimic various phenomena that happen in the interplay between general relativity and quantum field theory such as in black holes and the early Universe. The aim is for devising experiments of real laboratory tests that provide insights in phenomena and further probe the structure of curved-space quantum field theory. From a prospective of analog gravity, Unruh realized that sound waves in a moving fluid can be analogous to light waves in curved spacetime where the supersonic fluid can generate acoustic black holes with acoustic horizons [2]. Thus, the existence of analogous photonic Hawking radiation can be theoretically demonstrated. The work of Ref. [3] is a first experimental observation of Hawking radiation extracted from correlations of the collective excitations that agree with a thermal spectrum with the temperature estimated from analog surface gravity. Also, the time dependence of the Hawking radiation in an analog black hole is observed in Ref. [4].

With the advent of the experimental study of binary Bose-Einstein condensates (BECs) in Refs. [5,6], the condensates of cold atoms at zero temperature in such tunable systems have been explored with the Rabi transition between atomic hyperfine states where the system can be represented by a coupled two-field model of gapless excitations and gapped excitations. The binary BECs have been adopted as an analog model to theoretically mimic quantum phenomena in the early Universe and/or black holes [7–10]. In our previous work [10] we set up the configuration of the supersonic and subsonic regimes with constant flow velocity where the acoustic horizon is established between them in the elongated two-component BECs, trying to stimulate analogous Hawking radiation, in particular due to the gapped excitations. In this work, we consider the same model where the sound speed and flow velocity profiles are spatial dependent to generate the acoustic horizon with reference to the experiments in Refs. [3,11] and the theoretical studies in Refs. [12,13].

*syuweican@gmail.com
†dslee@gms.ndhu.edu.tw

Here we briefly review in what conditions of the coupling constants and condensate wave functions of the spatial dependence two collective excitations can be decoupled by following the work of Ref. [7]. We then consider the dispersion relation of the gapped modes with the k^2 term in a very long wavelength approximation that behaves relativistically. Some profiles of the spatial-dependent sound speed and the flow velocity are specified where the approximate analytic solutions of the mode equations of the gapped excitations can be treatable. The Unruh state is introduced as the appropriate state for the description of gravitational collapse of the black hole. The particle spectrum of the outgoing modes and their correlators are computed from which to further discuss the relevance to the experimental measurements.

We organize this paper as follows. In Sec. II, we introduce the model of a binary BEC system and give a review of the approach to decouple the gapless and gapped excitations. The particular sound speed and flow velocity profiles later are introduced to establish the acoustic horizon of the black hole. In addition, various asymptotic modes are identified. In Sec. III, the approximate analytical solution to the mode equations of the gapped excitations of interest is found from which the reflection and transmission coefficients for each scattering process are obtained. Also, the Unruh state is introduced. In Sec. IV, the field of the gapped excitations is expanded in terms of either incoming or outgoing modes whereas the corresponding S-matrix and the Bogoliubov transformations of the creation and annihilation operators between the incoming and outgoing modes are constructed. Section V is devoted to obtaining the particle density of outgoing modes and their correlators. We conclude the work in Sec. VI.

II. REVIEW OF MODE DECOUPLING IN TWO-COMPONENT BECs

The effective mass term of the quantum field theory can be considered as the gapped energy term of the gapped excitations in a binary BEC system in the hydrodynamic approximation [7,8,10]. Here we consider the binary BECs of the same atoms in two different internal hyperfine states. This class of the two-component BEC systems with the Rabi interaction exhibits two types of excitation on condensates: the gapless excitations due to the "in-phase" oscillations between two respective density waves and the gapped excitation stemming from the "out-of-phase" oscillations of the density waves with additional the Rabi transition, which are respectively analogous of the Goldstone modes and the Higgs modes in particle physics. Here we briefly review how two excitations are decoupled under certain conditions of the spatial-dependent condensate wave functions and the coupling constants [7]. With the unit $\hbar = k_{\mathrm{B}} = 1$ throughout this paper, the time-dependent equations of motion in $1+3$ dimensions are expressed by

$$i\partial_t\hat{\Psi}_1 = \left[-\frac{1}{2m}\vec{\nabla}^2 + V_1(\vec{x}) + g_{11}\hat{\Psi}_1^\dagger\hat{\Psi}_1 + g_{12}\hat{\Psi}_2^\dagger\hat{\Psi}_2\right] \times \hat{\Psi}_1 - \frac{\Omega}{2}\hat{\Psi}_2, \tag{1a}$$

$$i\partial_t\hat{\Psi}_2 = \left[-\frac{1}{2m}\vec{\nabla}^2 + V_2(\vec{x}) + g_{22}\hat{\Psi}_2^\dagger\hat{\Psi}_2 + g_{12}\hat{\Psi}_1^\dagger\hat{\Psi}_1\right] \times \hat{\Psi}_2 - \frac{\Omega}{2}\hat{\Psi}_1, \tag{1b}$$

where m is atomic mass and V_1 and V_2 are the external potentials on the hyperfine states 1 and 2, respectively. Additionally, g_{11}, g_{22}, and g_{12} are the interaction strengths of atoms between the same hyperfine states and different hyperfine states, respectively. The coupling strengths are related with the scattering lengths. Experimentally, the values of scattering lengths can be tuned using Feshbach resonances such as two hyperfine states of ^{87}Rb [14–17]. We also introduce a Rabi coupling term by shining the laser field or applying the radio wave with the strength given by the Rabi frequency Ω [18,19]. The condensate wave functions are given by the expectation value of the field operator $\langle\hat{\Psi}_i\rangle$:

$$\langle\hat{\Psi}_i\rangle = \sqrt{\rho_i}e^{i\theta_i - i\mu t} \tag{2}$$

with the chemical potential μ. The condensate flow velocities are given by $\vec{\nabla}\theta_i(x)/m = \vec{v}_i(x)$ $(i = 1, 2)$. The equations for ρ_i and θ_i of the condensate wave functions can be found in Refs. [7,9,10]. The perturbations around the stationary wave function are defined through

$$\hat{\Psi}_i = \langle\hat{\Psi}_i\rangle(1 + \hat{\phi}_i), \tag{3}$$

where the fluctuation fields in (3) can be decomposed in terms of the density and the phase as

$$\hat{\phi}_i = \delta\hat{n}_i + i\delta\hat{\theta}_i = \frac{\delta\hat{\rho}_i}{2\rho_i} + i\delta\hat{\theta}_i. \tag{4}$$

Substitutions of (3) and (4) into (1) give the coupled equations of two states 1 and 2. For the general spatial-dependent condensate wave functions as well as the coupling strengths, it is found that the above equations can be decoupled by choosing $\rho_1 = \rho_2 = \rho$, $\theta_1 = \theta_2 = \theta$, and $g_{11} = g_{22} = g$ [7]. The chosen scattering parameters in the binary systems can have a miscible state of background condensates [20,21]. The detailed analysis of the choice of the parameters can be found in our previous work [22]. One can therefore define

$$\delta\hat{n}_{d/p} = \frac{1}{\sqrt{2}}(\delta\hat{n}_1 \pm \delta\hat{n}_2), \tag{5a}$$

$$\delta\hat{\theta}_{d/p} = \frac{1}{\sqrt{2}}(\delta\hat{\theta}_1 \pm \delta\hat{\theta}_2), \tag{5b}$$

where the subscript d (p) refers to the density (polarization) fluctuations. The decoupled equations are shown to be

$$\partial_t \delta\hat{\theta}_d = \frac{1}{2m\rho}\overrightarrow{\nabla}\cdot(\rho\overrightarrow{\nabla}\delta\hat{n}_d) - \vec{v}\cdot\overrightarrow{\nabla}\delta\hat{\theta}_d - 2(g+g_{12})\rho\delta\hat{n}_d, \tag{6a}$$

$$\partial_t \delta\hat{n}_d = -\frac{1}{2m\rho}\overrightarrow{\nabla}\cdot(\rho\overrightarrow{\nabla}\delta\hat{\theta}_d) - \vec{v}\cdot\overrightarrow{\nabla}\delta\hat{n}_d, \tag{6b}$$

and

$$\partial_t \delta\hat{\theta}_p = \frac{1}{2m\rho}\overrightarrow{\nabla}\cdot(\rho\overrightarrow{\nabla}\delta\hat{n}_p) - \vec{v}\cdot\overrightarrow{\nabla}\delta\hat{\theta}_p - [2(g-g_{12})\rho + \Omega]\delta\hat{n}_p, \tag{7a}$$

$$\partial_t \delta\hat{n}_p = -\frac{1}{2m\rho}\overrightarrow{\nabla}\cdot(\rho\overrightarrow{\nabla}\delta\hat{\theta}_p) - \vec{v}\cdot\overrightarrow{\nabla}\delta\hat{n}_p + \Omega\delta\hat{\theta}_p. \tag{7b}$$

The analog Hawking radiation arising from the gapless modes has been studied in the literature [23–26]. Here we mainly focus on the gapped modes given by the polarization excitations in (7) where from now on the subscript p is dropped out for simplifying the notation. In this paper, we consider the transonic flow, which is accelerated by manipulating the condensate density $\rho(x)$ with the spatial dependence obtained from a sharp external potential [3,11] and spatial-dependent interaction strength $g_{12}(x)$. The experimentally spatial variation of the interaction strengths is challenging but feasible [27–29].

One thus combines (7a) and (7b) to obtain

$$-\left(\partial_t + \overrightarrow{\nabla}\vec{v}\right)\frac{\rho}{mc^2}\left(\partial_t + \vec{v}\overrightarrow{\nabla}\right)\delta\hat{\theta} + \overrightarrow{\nabla}\frac{\rho}{m}\overrightarrow{\nabla}\delta\hat{\theta} - 2\rho\Omega\delta\hat{\theta} = 0 \tag{8}$$

with the spatial-dependent sound speed $c(x) = \sqrt{[(g-g_{12})\rho(x)+\Omega]/m}$. To further express (8) as the form of the Klein-Gordon equation, the equation can be rewritten as

$$\left(\Box - \frac{mm_{\text{eff}}^2}{\rho c}\right)\delta\hat{\theta} = \frac{1}{\sqrt{-\mathbf{g}}}\partial_\mu\left(\sqrt{-\mathbf{g}}\mathbf{g}^{\mu\nu}\partial_\nu\delta\hat{\theta}\right) - \frac{mm_{\text{eff}}^2}{\rho c}\delta\hat{\theta} = 0 \tag{9}$$

with the gapped energy $m_{\text{eff}}(x) = \sqrt{2(g-g_{12})\rho(x)\Omega+\Omega^2} = \sqrt{2mc^2(x)\Omega}$. The acoustic metric is

$$ds^2 = \frac{\rho}{mc}[-(c^2-v^2)dt^2 - 2\vec{v}\cdot d\vec{x}dt + dx^2 + dy^2 + dz^2], \tag{10}$$

where we choose the direction of the flow along the x direction, $\vec{v}(x) = -v(x)\hat{x}$ $[v(x) > 0]$. It is then assumed that the system can be treated in the pseudo-one-dimension by applying a strong cigar-shape trap potential where the size of the trap L_x along the axial direction, say in the x direction, is much larger than the size of L_r along the radial direction [6,20,21]. Later, we will choose the profile of the sound speed and the flow velocity so that the Klein-Gordon equation can be treatable analytically in some approximations to be discussed later [12,30,31]. Using the transformation to define the time τ from the laboratory time t as

$$\tau = t - \int dx\frac{v}{c^2 - v^2} \tag{11}$$

to rewrite the metric (10) restricted in one dimension along the x direction as

$$ds^2 = \frac{\rho}{mc}\left[-(c^2-v^2)d\tau^2 + \frac{c^2}{c^2-v^2}dx^2\right], \tag{12}$$

the corresponding Klein-Gordon equation becomes

$$\left[\frac{-c}{\rho(c^2-v^2)}\partial_\tau^2 + \partial_x\left(\frac{c^2-v^2}{\rho c}\partial_x\right) - \frac{m_{\text{eff}}^2}{\rho c}\right]\delta\hat{\theta}(x,\tau) = 0. \tag{13}$$

According to Ref. [12], we perform the further variable transformation

$$dx = \frac{1}{\rho}\left(1 - \frac{v^2}{c^2}\right)dz, \tag{14}$$

giving the metric

$$ds^2 = \frac{\rho}{mc}(c^2-v^2)\left[-d\tau^2 + \frac{1}{\rho^2c^2}dz^2\right]. \tag{15}$$

We further use the continuity equation of the gapped excitations $v\rho = \text{const}$ resulting from the respective continuity equations for states 1 and 2 with equal phases and densities between them to set $\rho = 1/v$ and rewrite (13) to be

$$\left[\frac{v^2}{c^2}\partial_\tau^2 - \partial_z^2 + v^2\left(1 - \frac{v^2}{c^2}\right)2m\Omega\right]\delta\hat{\theta}(z,\tau) = 0. \tag{16}$$

The third term of (16) is induced by the gap energy, giving the analog mass term of the relativistic quantum scalar field. The mass term is positive (negative) in the subsonic (supersonic) region, which implies that there will exist the threshold frequency in the subsonic region beyond which to have the propagating modes [32,33].

In the supersonic region ($v > c$), we assume that the sound speed and the flow velocity have the forms [12,13]

$$c_{\rm sup}(z) = \left[\frac{c_l^{-2}+v_0^{-2}}{2} + \frac{(c_l^{-2}-v_0^{-2})}{2}\tanh(\kappa z)\right]^{-1/2}, \quad (17a)$$

$$v_{\rm sup}(z) = \left[\frac{v_l^{2}+v_0^{2}}{2} + \frac{(v_l^{2}-v_0^{2})}{2}\tanh(\kappa z)\right]^{1/2} \quad (17b)$$

with the asymptotic behaviors $(v_{\rm sup}, c_{\rm sup})_{z\to\infty} \to (v_l, c_l)$ for $x \to -\infty$ and $(v_{\rm sup}, c_{\rm sup})_{z\to-\infty} \to (v_0, v_0)$ for $x \to 0$ of the horizon given from the spatial coordinate transformation (14). In the subsonic region ($c > v$), they are assumed to be

$$c_{\rm sub}(z) = \left[\frac{c_r^{-2}+v_0^{-2}}{2} + \frac{(c_r^{-2}-v_0^{-2})}{2}\tanh(\kappa z)\right]^{-1/2}, \quad (18a)$$

$$v_{\rm sub}(z) = \left[\frac{v_r^{2}+v_0^{2}}{2} + \frac{(v_r^{2}-v_0^{2})}{2}\tanh(\kappa z)\right]^{1/2}, \quad (18b)$$

where $(v_{\rm sub}, c_{\rm sub})_{z\to\infty} \to (v_r, c_r)$ for $x \to +\infty$ and $(v_{\rm sub}, c_{\rm sub})_{z\to-\infty} \to v_0$ for $x \to 0$ of the horizon again from (14). The horizon from the transonic flow with the above profile is formed by manipulating the phonon sound speed and the flow velocity with the experimentally accessible parameters [3,11]. In Fig. 1, we show the transonic transition according to (17) and (18) under the transformation (14). Thus, in the asymptotical regions, the velocities reach respective constants where the metric (15) is conformal to that of the Minkowski spacetime with the spatial coordinate in terms of the rescaled vdz/c. One can define the incoming and outgoing states in these asymptotic regions of the Penrose diagram shown in Ref. [12] and Fig. 2 in this paper. The location of the analog horizon is at $x = 0$ with the surface gravity

$$\kappa = \left.\frac{d(c-v)}{dx}\right|_{x=0} \quad (19)$$

that can be justified by substituting (14), (17), and (18) into (19).

With the profiles of a transonic flow (17) and (18), the solutions of (16) in the subsonic and supersonic regions separately can be cast in a form of $\delta\theta(\tau, z) = e^{-i\omega\tau}\varphi_\omega(z)$, to therefore rewrite (16) as

$$\omega^2 M_{\rm a}^2(z)\eta_{\rm a}^2(z)\varphi_\omega^{\rm a}(z) + \frac{d^2\varphi_\omega^{\rm a}(z)}{dz^2} = 0, \quad (20)$$

where the index "a" refers to "sup" or "sub" for different regions. The quantity $\eta_{\rm a}(z)$ is defined as

$$\eta_{\rm a}(z) = \sqrt{1-(\pm)_{\rm a}\frac{\omega_{\rm a}^2(z)}{\omega^2}} \quad (21)$$

with

$$\omega_{\rm a}^2(z) \equiv 2m|c_a^2(z) - v_a^2(z)|\Omega, \quad (22)$$

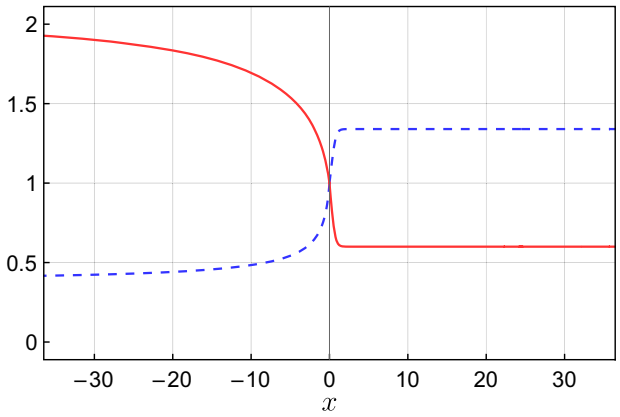

FIG. 1. Profiles of the sound speed $c(x)$ (blue dashed line) and the flow velocity $v(x)$ (solid red line) are depicted from (17) and (18) with parameters $c_l = 0.4$, $v_l = 2$, $c_r = 1.34$, and $v_r = 0.6$ with the reference value $v_0 = 1$ at the horizon. The Mach numbers are chosen to be $M_l = 5$ and $M_r = 0.44$, where $M_r = 1/\sqrt{M_l}$ with reference to Refs. [13,26,34].

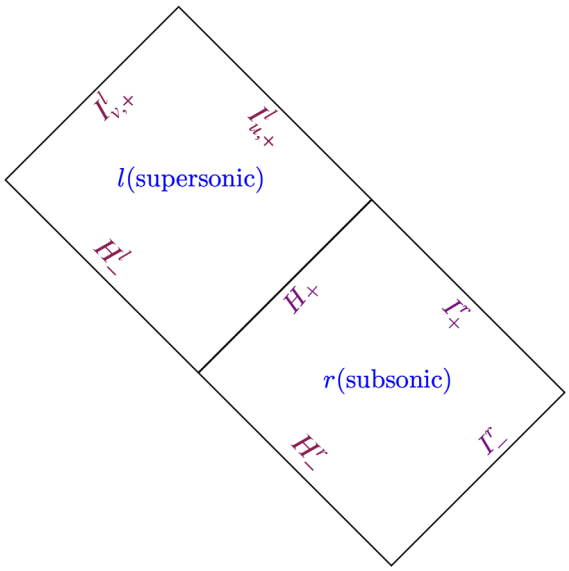

FIG. 2. Schematic plot of the Penrose diagram.

where + (−) is for the subsonic (supersonic) region. We also express (20) in terms of the Mach number defined by

$$M_{\rm a}(z) = \frac{v_{\rm a}(z)}{c_{\rm a}(z)}. \quad (23)$$

As a result of the asymptotic behaviors of (18) and (17), the function η_a and ω_a will be saturated to a constant value in the asymptotic regions where we summarize them as

$$\begin{cases} \eta_{\rm sub} \to \eta_r = \sqrt{1-\omega_r^2/\omega^2} \\ \omega_{\rm sub} \to \omega_r = \sqrt{2mc_r^2(1-M_r^2)\Omega} \quad \text{for } z \to \infty, \\ M_{\rm sub} \to M_r = v_r/c_r \end{cases} \quad (24a)$$

$$\begin{cases} \eta_{\rm sub} \to 1 \\ \omega_{\rm sub} \to 0 \\ M_{\rm sub} \to 1 \end{cases} \quad \text{for } z \to -\infty \tag{24b}$$

in the subsonic region and

$$\begin{cases} \eta_{\rm sup} \to \eta_l = \sqrt{1+\omega_l^2/\omega^2} \\ \omega_{\rm sup} \to \omega_l = \sqrt{2mc_l^2(M_l^2-1)\Omega} \\ M_{\rm sup} \to M_l = v_l/c_l \end{cases} \quad \text{for } z \to \infty, \tag{25a}$$

$$\begin{cases} \eta_{\rm sup} \to 1 \\ \omega_{\rm sup} \to 0 \\ M_{\rm sup} \to 1 \end{cases} \quad \text{for } z \to -\infty \tag{25b}$$

in the supersonic region.

To make (20) analytically treatable, we approximate the first term of (20) in a form

$$(M^2\eta^2)_{\rm sub/\,sup} \simeq \frac{1}{2}[M_{r/l}^2\eta_{r/l}^2 + 1 + (M_{r/l}^2\eta_{r/l}^2 - 1) \times \tanh(\kappa(z+\delta z_{\rm sub/\,sup}))] \tag{26}$$

with the shift

$$\delta z_{\rm sub/sup} = \frac{\left[(v_0^2 - v_{r/l}^2)(c_{r/l}^2 - v_0^2)\right]\left[2\omega^2 + (3v_0^2 + v_{r/l}^2)2m\Omega\right]}{4v_0^2(c_{r/l}^2 - v_{r/l}^2)(\omega^2 + v_{r/l}^2 2m\Omega)}, \tag{27}$$

that the parametrized function matches not only at the asymptotical values but also at $z = 0$ (see Fig. 3), although the shift does not affect the behaviors of the scattering processes asymptotically. Based upon the asymptotic regions of the Penrose diagram (see Fig. 2), there are three

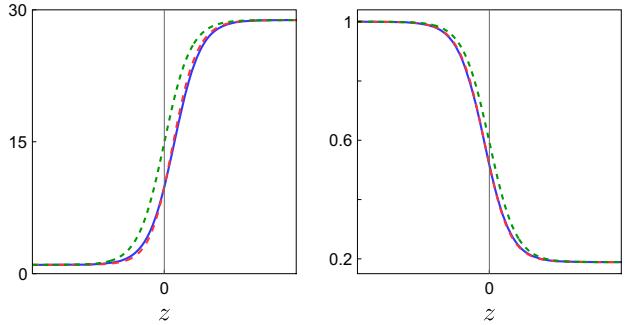

FIG. 3. Comparison of the exact $M^2(z)\eta^2(z)$ (blue line) in (20) computed from the sound speed and the flow velocity in (17) and (18) and the parametrized function (26) with (red dashed line) and without (green dotted line) shift (27) in the supersonic (left panel) and subsonic regions (right panel).

incoming modes coming from the past horizon in the right (left) of the horizon H_-^r (H_-^l) of the subsonic (supersonic) region and the past null infinity I_- in the subsonic region with the following mode functions:

$$e^{-i\omega\tau}\varphi_{\omega,H}^{{\rm in},r}(z) = \sqrt{\frac{1}{4\pi\omega}}e^{-i\omega\tau}e^{i\omega z} \quad \text{from } H_-^r, \tag{28}$$

$$e^{i\omega\tau}\varphi_{\omega,H}^{{\rm in},l}(z) = \sqrt{\frac{1}{4\pi\omega}}e^{i\omega\tau}e^{-i\omega z} \quad \text{from } H_-^l, \tag{29}$$

$$e^{-i\omega\tau}\varphi_{\omega,I}^{{\rm in},r}(z) = \sqrt{\frac{1}{4\pi\omega M_r\eta_r}}e^{-i\omega\tau}e^{-i\omega M_r\eta_r z} \quad \text{from } I_-^r. \tag{30}$$

In the case of the metric given in (15), the mode functions shown above in the subsonic region ($v < c$) correspond to the positive frequency modes with respect to the time coordinate τ whereas the mode functions in the supersonic region ($v > c$) are the positive frequency modes with respect to the "time" coordinate z. According to (20), the normalization of the mode functions $\varphi_\omega^{\rm in}(z)$ as well as its frequency dependence of the mode functions can be chosen from the standard one $\varphi_\omega^{\rm in}(z) = \frac{1}{\sqrt{4\pi\omega}}e^{\pm i\omega z}$ by replacing $\omega \to \omega M_{\rm a}\eta_{\rm a}$ evaluated either at the horizon or the past null infinity, which is consistent with Refs. [12,30,35]. Similarly, there are three outgoing modes. They are u_l and v_l modes in the supersonic region toward the future null infinity in the respective asymptotic regions in terms of the incoming and outgoing null coordinates $v_l = \tau + M_l z$ and $u_l = \tau - M_l z$ realized from the metric form (15). Also, in the subsonic region, the $u_r = \tau - M_r z$ mode is involved. The mode functions are

$$e^{-i\omega\tau}\varphi_{\omega,u_r}^{{\rm out},r}(z) = \sqrt{\frac{1}{4\pi\omega M_r\eta_r}}e^{-i\omega\tau}e^{i\omega M_r\eta_r z} \quad \text{toward } I_+^r, \tag{31}$$

$$e^{i\omega\tau}\varphi_{\omega,u_l}^{{\rm out},l}(z) = \sqrt{\frac{1}{4\pi\omega M_l\eta_l}}e^{i\omega\tau}e^{-i\omega M_l\eta_l z} \quad \text{toward } I_{u,+}^l, \tag{32}$$

$$e^{-i\omega\tau}\varphi_{\omega,v_l}^{{\rm out},l}(z) = \sqrt{\frac{1}{4\pi\omega M_l\eta_l}}e^{-i\omega\tau}e^{-i\omega M_l\eta_l z} \quad \text{toward } I_{v,+}^l. \tag{33}$$

Notice that the correct choice of the normalization of the mode functions becomes essential to fulfill the unitarity conditions to be checked later. The detailed mode functions will be determined in the next section.

III. SOLUTIONS OF THE MODE EQUATIONS

A. Incoming mode $\theta_H^{{\rm in},r}$

Firstly, we consider the incoming mode $\theta_H^{{\rm in},r}$ from the right region of the past horizon for $\omega > \omega_r$ by evaluating

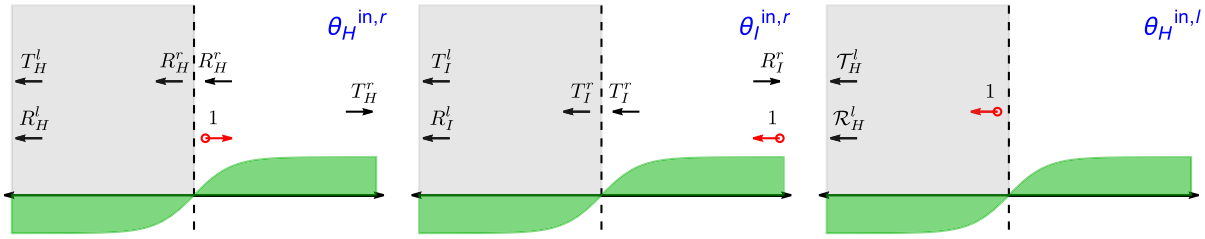

FIG. 4. Scattering processes of the incoming mode $\theta_H^{\text{in},r}$ (left), $\theta_I^{\text{in},r}$ (middle), and $\theta_H^{\text{in},l}$ (right). According to (22), the green shadow is depicted for $+\omega_{\text{sub}}^2(z)$ in the subsonic region and $-\omega_{\text{sup}}^2(z)$ in the supersonic region.

the threshold frequency ω_{sub} in the past horizon in the subsonic region shown in (24) (see Fig. 2), which then partially reflects back to the future horizon with the amplitude R_H^r and partially transmits with the amplitude T_H^r toward the future null infinity in the subsonic region I_+^r. However, for $\omega < \omega_r$, the incident mode will be totally reflected giving $T_H^r = 0$ and $R_H^r = 1$ toward the future horizon, which is referred as the boomerang trajectory of the gapped excitations [33]. The scattering process can be schematically shown in Fig. 4 (left) with the asymptotic behaviors of the mode function in a subsonic region ($x > 0$) given by

$$\varphi_{\omega,H}^{\text{in},r}(z) = \begin{cases} \sqrt{\frac{1}{4\pi\omega}}\exp(i\omega z) + R_H^r\sqrt{\frac{1}{4\pi\omega}}\exp(-i\omega z), & z \to -\infty. \\ T_H^r\sqrt{\frac{1}{4\pi\omega M_r\eta_r}}\exp(i\omega M_r\eta_r z), & z \to \infty. \end{cases} \tag{34}$$

The scattering coefficients in (34) can be found from the approximate solution of (20) with the parametrization function (26) together with the asymptotic values of $M_{\text{sub}}\eta_{\text{sub}}$ (24). We choose one of two independent solutions given by

$$\varphi_\omega^{\text{sub}}(z) \propto e^{-\frac{\pi\omega}{2\kappa}}(-e^{\kappa\delta z_{\text{sub}}})^{\frac{i\omega}{\kappa}}(e^{\kappa z})^{\frac{i\omega}{\kappa}}(e^{2\kappa(z+\delta z_{\text{sub}})}+1)^{\frac{i(1-M_r\eta_r)\omega}{2\kappa}} \times {}_2F_1(a,b;c;y), \tag{35}$$

where ${}_2F_1$ is the hypergeometric function with the arguments

$$a = \frac{i}{2}\frac{(1+M_r\eta_r)\omega}{\kappa}, \tag{36a}$$

$$b = 1 - \frac{i}{2}\frac{(1-M_r\eta_r)\omega}{\kappa}, \tag{36b}$$

$$c = 1 + \frac{iM_r\eta_r\omega}{\kappa}, \tag{36c}$$

$$y = \frac{1}{1+e^{2\kappa(z+\delta z_{\text{sub}})}}, \tag{36d}$$

with $M_r\eta_r$ in (24). Since the hypergeometric function ${}_2F_1(a,b,c;y=0)=1$ in the case of $1/(1+e^{2\kappa(z+\delta z_{\text{sub}})})\to 0$ as $z \to \infty$, the amplitude in (35) becomes an outgoing mode:

$$\varphi_\omega^{\text{sub}}(z) \propto e^{i\omega M_r\eta_r z} \quad \text{as } z \to \infty. \tag{37}$$

Furthermore, near the horizon ($z \to -\infty$), we use the identity

$$\begin{aligned} {}_2F_1(a,b;c;y) = {} & \frac{\Gamma(c)\Gamma(c-a-b)}{\Gamma(c-a)\Gamma(c-b)} \\ & \times {}_2F_1(a,b;a+b+1-c;1-y) \\ & + \frac{\Gamma(c)\Gamma(a+b-c)}{\Gamma(a)\Gamma(b)}(1-y)^{c-a-b} \\ & \times {}_2F_1(c-a,c-b;1+c-a-b;1-y) \end{aligned} \tag{38}$$

to rewrite (35) as

$$\varphi_\omega^{\text{sub}}(z) \propto \frac{\Gamma(c)\Gamma(c-a-b)}{\Gamma(c-a)\Gamma(c-b)}e^{i\omega z} + \frac{\Gamma(c)\Gamma(a+b-c)}{\Gamma(a)\Gamma(b)}e^{-i\omega z} \quad \text{as } z \to -\infty \tag{39}$$

with ${}_2F_1(a,b,c;1-y=0)=1$ again since $1-y = e^{2\kappa z}/(1+e^{2\kappa z}) \to 0$ for $z \to -\infty$. Comparing (34), (37) and (39), we are able to extract the reflection coefficient R_H^r and the transmission coefficient T_H^r obtained as

$$R_H^r = \frac{\Gamma(c-a)\Gamma(c-b)\Gamma(a+b-c)}{\Gamma(a)\Gamma(b)\Gamma(c-a-b)}, \tag{40}$$

$$T_H^r = \sqrt{M_r\eta_r}\frac{\Gamma(c-a)\Gamma(c-b)}{\Gamma(c)\Gamma(c-a-b)}. \tag{41}$$

Consequently they are

$$T_H^r = \sqrt{M_r\eta_r}\frac{\Gamma\left(\frac{i(1+M_r\eta_r)\omega}{2k}\right)\Gamma\left(1+\frac{i(1+M_r\eta_r)\omega}{2k}\right)}{\Gamma(\frac{i\omega}{k})\Gamma\left(1+\frac{iM_r\eta_r\omega}{k}\right)}\theta(\omega-\omega_r), \tag{42}$$

$$R_H^r = \frac{\Gamma(-\frac{i\omega}{\kappa})\Gamma\left(\frac{i(1+M_r\eta_r)\omega}{2\kappa}\right)\Gamma\left(1+\frac{i(1+M_r\eta_r)\omega}{2\kappa}\right)}{\Gamma(\frac{i\omega}{\kappa})\Gamma\left(-\frac{i(1-M_r\eta_r)\omega}{2\kappa}\right)\Gamma\left(1-\frac{i(1-M_r\eta_r)\omega}{2\kappa}\right)}, \qquad \omega > \omega_r, \tag{43a}$$

$$= 1, \qquad \omega \le \omega_r, \tag{43b}$$

which satisfy the unitarity relation

$$|R_H^r|^2 + |T_H^r|^2 = 1. \tag{44}$$

In (42), $\theta(\omega-\omega_r)$ is the Heaviside step function. Afterward, the mode function with the amplitude R_H^r that propagates from the subsonic region to the supersonic region transmits (reflects) to the future null infinity in the supersonic region as in terms of the v (u) mode with the following asymptotic behaviors:

$$\varphi_{\omega,H}^{\text{in},r} = \begin{cases} R_H^r\sqrt{\frac{1}{4\pi\omega}}\exp(i\omega z), & z\to-\infty, \\ T_H^l\sqrt{\frac{1}{4\pi\omega M_l\eta_l}}\exp(-i\omega M_l\eta_l z) + R_H^l\sqrt{\frac{1}{4\pi\omega M_l\eta_l}}\exp(i\omega M_l\eta_l z), & z\to\infty. \end{cases} \tag{45}$$

For the supersonic region, the solution has the general solution

$$\varphi_\omega^{\sup}(z) \propto e^{-\frac{\pi\omega}{2\kappa}}(-e^{\kappa\delta z})^{\frac{i\omega}{\kappa}}(e^{\kappa z})^{\frac{i\omega}{\kappa}}(e^{(\kappa(z+\delta z_{\sup}))}+1)^{-\frac{i(M_l\eta_l-1)\omega}{\kappa}} \times {}_2F_1(a,b;c;y) \tag{46}$$

with the arguments

$$a = -\frac{i}{2}\frac{(M_l\eta_l-1)\omega}{\kappa}, \tag{47a}$$

$$b = 1-\frac{i}{2}\frac{(M_l\eta_l-1)\omega}{\kappa}, \tag{47b}$$

$$c = 1+\frac{i\omega}{\kappa}, \tag{47c}$$

$$y = \frac{1}{1+e^{-2\kappa(z+\delta z)}}, \tag{47d}$$

where $M_l\eta_l$ is in (25). For $z\to-\infty$, giving $y\to 0$, where ${}_2F_1(a,b;c;0)=1$, the solution (46) correctly describes the incident wave from the future horizon as

$$\varphi_\omega^{\sup}(z) \propto e^{-i\omega z} \quad \text{as } z\to-\infty. \tag{48}$$

However, for $z\to\infty$, we use the transformation (38) to rewrite (46) as

$$\varphi_\omega^{\sup}(z) \propto \frac{\Gamma(c)\Gamma(c-a-b)}{\Gamma(c-a)\Gamma(c-b)}e^{-i\omega\eta_l M_l z} + \frac{\Gamma(c)\Gamma(a+b-c)}{\Gamma(a)\Gamma(b)} \times e^{i\omega\eta_l M_l z} \quad \text{as } z\to\infty. \tag{49}$$

Comparing (45) and (49) enables us to extract the scattering coefficients

$$T_H^l = \sqrt{M_l\eta_l}\frac{\Gamma(1+\frac{i\omega}{\kappa})\Gamma(\frac{iM_l\eta_l\omega}{\kappa})}{\Gamma\left(\frac{i(M_l\eta_l+1)\omega}{2\kappa}\right)\Gamma\left(1+\frac{i(M_l\eta_l+)\omega}{2\kappa}\right)}R_H^r, \tag{50}$$

$$R_H^l = \sqrt{M_l\eta_l}\frac{\Gamma(1+\frac{i\omega}{\kappa})\Gamma\left(-\frac{i\omega M_l\eta_l}{\kappa}\right)}{\Gamma\left(-\frac{i\omega(M_l\eta_l-1)}{2\kappa}\right)\Gamma\left(1-\frac{i\omega(M_l\eta_l-1)}{2\kappa}\right)}R_H^r. \tag{51}$$

For the whole scattering process from the mode function $\varphi_{\omega,H}^{\text{in},r}(z)$, the above coefficients satisfy the relation

$$|T_H^l|^2 - |R_H^l|^2 + |T_H^r|^2 = 1, \tag{52}$$

where the minus sign is due to the negative norm of the reflected u mode in the supersonic region.

B. Incoming mode $\theta_I^{\text{in},r}$

The second incoming propagating mode $\theta_I^{\text{in},r}$ is also considered for $\omega>\omega_r$ from past null infinity I_-^r in the subsonic region, which scatters into the reflected mode with the reflection coefficient R_I^r in the future null infinity, and the transmitted mode with the transmission coefficient T_I^r toward the future horizon [see Figs. 2 and 4 (middle)].

The incoming mode $\theta_I^{\text{in},r}(\tau,z)$ has the asymptotic forms in the subsonic region as

$$\varphi_{\omega,I}^{\text{in},r}=\begin{cases} T_I^r\sqrt{\frac{1}{4\pi\omega}}\exp\left(-i\omega z\right), & z\to-\infty,\\ \sqrt{\frac{1}{4\pi\omega M_r\eta_r}}\exp\left(-i\omega M_r\eta_r z\right)+R_I^r\sqrt{\frac{1}{4\pi\omega M_r\eta_r}}\exp\left(i\omega M_r\eta_r z\right), & z\to\infty. \end{cases} \tag{53}$$

Then, in the supersonic region, the mode with the amplitude T_I^r coming from the future horizon scatters into the transmitted (reflected) mode to the future null infinity in the supersonic region in terms of the v (u) mode with the following asymptotic behaviors:

$$\varphi_{\omega,I}^{\text{in},r}=\begin{cases} T_I^r\sqrt{\frac{1}{4\pi\omega}}\exp\left(-i\omega z\right), & z\to-\infty,\\ T_I^l\sqrt{\frac{1}{4\pi\omega M_l\eta_l}}\exp\left(-i\omega M_l\eta_l z\right)+R_I^l\sqrt{\frac{1}{4\pi\omega M_l\eta_l}}\exp\left(i\omega M_l\eta_l z\right), & z\to\infty. \end{cases} \tag{54}$$

Following the same procedure as in Sec. III A to match the incoming mode $\varphi_{\omega,I}^{\text{in},r}$ of the solutions with the mode function $\varphi_\omega^{\text{sub/ sup}}$ near the horizon and the asymptotic regions, one obtains the scattering coefficients

$$T_I^r=\frac{\Gamma\left(\frac{i(M_r\eta_r+1)\omega}{2\kappa}\right)\Gamma\left(1+\frac{i(M_r\eta_r+1)\omega}{2\kappa}\right)}{\sqrt{M_r\eta_r}\Gamma\left(1+\frac{i\omega}{\kappa}\right)\Gamma\left(\frac{i\omega M_r\eta_r}{\kappa}\right)}\theta(\omega-\omega_r), \tag{55}$$

$$R_I^r=\frac{\Gamma\left(-\frac{i\omega M_r\eta_r}{\kappa}\right)\Gamma\left(\frac{i(1+M_r\eta_r)\omega}{2\kappa}\right)\Gamma\left(1+\frac{i(1+M_r\eta_r)\omega}{2\kappa}\right)}{\Gamma\left(\frac{i\omega M_r\eta_r}{\kappa}\right)\Gamma\left(-\frac{i(M_r\eta_r-1)\omega}{2\kappa}\right)\Gamma\left(1-\frac{i(M_r\eta_r-1)\omega}{2\kappa}\right)}\theta(\omega-\omega_r), \tag{56}$$

$$R_I^l=\sqrt{M_l\eta_l}\frac{\Gamma\left(1+\frac{i\omega}{\kappa}\right)\Gamma\left(-\frac{i\omega M_l\eta_l}{\kappa}\right)}{\Gamma\left(-\frac{i(M_l\eta_l-1)\omega}{2\kappa}\right)\Gamma\left(1-\frac{i(M_l\eta_l-1)\omega}{2\kappa}\right)}T_I^r, \tag{57}$$

$$T_I^l=\sqrt{M_l\eta_l}\frac{\Gamma\left(1+\frac{i\omega}{\kappa}\right)\Gamma\left(\frac{i\omega M_l\eta_l}{\kappa}\right)}{\Gamma\left(\frac{i(M_l\eta_l+1)\omega}{2\kappa}\right)\Gamma\left(1+\frac{i(M_l\eta_l+1)\omega}{2\kappa}\right)}T_I^r. \tag{58}$$

These coefficients obey the relations

$$|R_I^r|^2+|T_I^r|^2=1, \tag{59}$$

$$|T_I^l|^2-|R_I^l|^2+|R_I^r|^2=1. \tag{60}$$

Notice that this scattering process can only happen as $\omega>\omega_r$. Again, the negative norm of the reflected u mode in the supersonic region gives the minus sign in the equation.

C. Incoming mode $\theta_H^{\text{in},l}$

The third incoming mode under consideration is $\theta_H^{\text{in},l}$, which is incident from the past horizon in the supersonic region. As seen in Figs. 2 and 4 (right), we have one partial reflected mode, in particular of the negative norm state accompanying with reflection coefficient $\mathcal{R}_H^l$, and one partial transmitted mode with the transmission coefficient $\mathcal{T}_H^l$. Note that this scattering process has nothing to do with the subsonic region due to the formation of the analog horizon where the modes are forced to travel toward $x\to-\infty$ away from the horizon and will not escape into the subsonic region.

The asymptotic behaviors of the incoming mode $\varphi_{\omega,H}^{\text{in},l}$ in the supersonic region are

$$\varphi_{\omega,H}^{\text{in},l}=\begin{cases} \sqrt{\frac{1}{4\pi\omega}}\exp\left(-i\omega z\right), & z\to-\infty,\\ \mathcal{T}_H^l\sqrt{\frac{1}{4\pi\omega M_l\eta_l}}\exp\left(-i\omega M_l\eta_l z\right)+\mathcal{R}_H^l\sqrt{\frac{1}{4\pi\omega M_l\eta_l}}\exp\left(i\omega M_l\eta_l z\right), & z\to\infty. \end{cases} \tag{61}$$

It is straightforward to obtain the scattering coefficients by letting $T_I^r=1$ in (57) and (58) as

$$\mathcal{R}_H^l=\sqrt{M_l\eta_l}\frac{\Gamma(1+\frac{i\omega}{\kappa})\Gamma\left(-\frac{i\omega M_l\eta_l}{\kappa}\right)}{\Gamma\left(-\frac{i\omega(M_l\eta_l-1)}{2\kappa}\right)\Gamma\left(1-\frac{i\omega(M_l\eta_l-1)}{2\kappa}\right)}, \tag{62}$$

$$\mathcal{T}_H^l = \sqrt{M_l\eta_l}\frac{\Gamma\left(1+\frac{i\omega}{\kappa}\right)\Gamma\left(\frac{i\omega M_l\eta_l}{\kappa}\right)}{\Gamma\left(\frac{i(M_l\eta_l+1)\omega}{2\kappa}\right)\Gamma\left(1+\frac{i(M_l\eta_l+1)\omega}{2\kappa}\right)}, \tag{63}$$

which satisfy the relation

$$|\mathcal{T}_H^l|^2 - |\mathcal{R}_H^l|^2 = 1. \tag{64}$$

In Ref. [12] where the gapless cases are under consideration, the scattering coefficients are shown only in the subsonic region where our results are consistent with them in the limit of $\eta_r \to 1(\Omega \to 0)$.

IV. CONSTRUCTION OF S-MATRIX AND BOGOLIUBOV TRANSFORMATION

Having all the scattering coefficients from all incoming modes, we are able to construct the mode expansion of the field operator in terms of incoming modes

$$\delta\hat{\theta}(\tau,z) = \int d\omega\Big\{e^{-i\omega\tau}\Big[\hat{a}^{\mathrm{in},r}_{\omega,H}\varphi^{\mathrm{in},r}_{\omega,H} + \hat{a}^{\mathrm{in},r}_{\omega,I}\varphi^{\mathrm{in},r}_{\omega,I} + (\hat{a}^{\mathrm{in},l}_{\omega,H})^\dagger\varphi^{\mathrm{in},l*}_{\omega,H}\Big] + \mathrm{H.c.}\Big\} \tag{65}$$

or in terms of outgoing modes

$$\delta\hat{\theta}(\tau,z) = \int d\omega\Big\{e^{-i\omega\tau}\Big[\hat{a}^{\mathrm{out},r}_{\omega,u_r}\varphi^{\mathrm{out},r}_{\omega,u_r} + \hat{a}^{\mathrm{out},l}_{\omega,v_l}\varphi^{\mathrm{out},l}_{\omega,v_l} + (\hat{a}^{\mathrm{out},l}_{\omega,u_l})^\dagger\varphi^{\mathrm{out},l*}_{\omega,u_l}\Big] + \mathrm{H.c.}\Big\}, \tag{66}$$

according to the asymptotic states defined on the boundaries of the Penrose diagram in Fig. 2. The relation between incoming and outgoing modes given by (28)–(33) can be summarized into the S matrix to be

$$\begin{pmatrix} \varphi^{\mathrm{in},r}_{\omega,H} \\ \varphi^{\mathrm{in},l*}_{\omega,H} \\ \varphi^{\mathrm{in},r}_{\omega,I} \end{pmatrix} = S\cdot\begin{pmatrix} \varphi^{\mathrm{out},r}_{\omega,u_r} \\ \varphi^{\mathrm{out},l*}_{\omega,u_l} \\ \varphi^{\mathrm{out},l}_{\omega,v_l} \end{pmatrix}, \tag{67}$$

where

$$S = \begin{pmatrix} S_{ur,Hr} & S_{ul,Hr} & S_{vl,Hr} \\ S_{ur,Hl} & S_{ul,Hl} & S_{vl,Hl} \\ S_{ur,Ir} & S_{ul,Ir} & S_{vl,Ir} \end{pmatrix}. \tag{68}$$

The subscript of the element $S_{i,j}$ indicates the relation between the i outgoing mode and the j incoming mode. Substituting (68) into (65) and comparing with (66), the Bogoliubov transformation can be read off as

$$\begin{pmatrix} \hat{a}^{\mathrm{out},r}_{\omega,u_r} \\ (\hat{a}^{\mathrm{out},l}_{\omega,u_l})^\dagger \\ \hat{a}^{\mathrm{out},l}_{\omega,v_l} \end{pmatrix} = \begin{pmatrix} S_{ur,Hr} & S_{ur,Hl} & S_{ur,Ir} \\ S_{ul,Hr} & S_{ul,Hl} & S_{ul,Ir} \\ S_{vl,Hr} & S_{vl,Hl} & S_{vl,Ir} \end{pmatrix}\cdot\begin{pmatrix} \hat{a}^{\mathrm{in},r}_{\omega,H} \\ (\hat{a}^{\mathrm{in},l}_{\omega,H})^\dagger \\ \hat{a}^{\mathrm{in},r}_{\omega,I} \end{pmatrix}, \tag{69}$$

where the S-matrix elements are related to all above transmission and reflection coefficients below:

$$S_{ur,Hr} = T^r_H, \qquad S_{ur,Hl} = 0, \qquad S_{ur,Ir} = R^r_I, \tag{70a}$$

$$S_{ul,Hr} = R^l_H, \qquad S_{ul,Hl} = \mathcal{T}^{l*}_H, \qquad S_{ul,Ir} = R^l_I, \tag{70b}$$

$$S_{vl,Hr} = T^l_H, \qquad S_{vl,Hl} = \mathcal{R}^{l*}_H, \qquad S_{vl,Ir} = T^l_I. \tag{70c}$$

When studying a physical effect of some quantum field in a curved spacetime, an important step is the identification of a quantum state or a class of quantum states which adequately describes the given physical situation. Based upon the mode expansion in (66) the natural vacuum state can be defined as the Boulware state, which is annihilated by the annihilation operators $\hat{a}^{\mathrm{in},r}_{\omega,I}$, $\hat{a}^{\mathrm{in},r}_{\omega,H}$ and $\hat{a}^{\mathrm{in},l}_{\omega,H}$, namely

$$\hat{a}^{\mathrm{in},r}_{\omega,I}|B\rangle = 0, \qquad \hat{a}^{\mathrm{in},r}_{\omega,H}|B\rangle = 0, \quad \text{and} \quad \hat{a}^{\mathrm{in},l}_{\omega,H}|B\rangle = 0. \tag{71}$$

Here we consider the Unruh state, a stationary state that can be thought of as describing a hot body, namely the black hole, immersed in vacuum. In particular, it contains no particles coming from the past null infinity, while at the future null infinity, the particles can be produced. This is consistent with blackbody radiation at the Hawking temperature. Thus the Unruh state is generally considered to be the appropriate state for the description of gravitational collapse of the black hole [2]. The positive and negative frequency modes of the Unruh state are defined with respect to the Kruskal time $U = \pm e^{-\kappa(\tau-z)}/\kappa$ where $+$ $(-)$ corresponds to the supersonic (subsonic) region of the horizon with the mode function

$$\varphi^K_H = \sqrt{\frac{1}{4\pi\omega_K}}e^{-i\omega_K U}. \tag{72}$$

Thus, the field operator can also be expanded in terms of the mode functions φ^K_H and $\varphi^{\mathrm{in},r}_I$:

$$\delta\hat{\theta} = \int d\omega_K(\hat{a}_{\omega_K}\varphi^K_H + \hat{a}^\dagger_{\omega_K}\varphi^{K*}_H) + \int d\omega\Big(\hat{a}^{\mathrm{in},r}_{\omega,I}\varphi^{\mathrm{in},r}_{\omega,I} + (\hat{a}^{\mathrm{in},r}_{\omega,I})^\dagger\varphi^{\mathrm{in},r*}_{\omega,I}\Big), \tag{73}$$

where the Unruh state is annihilated by the annihilation operators $\hat{a}_{\omega_K}$ and $\hat{a}^\dagger_{\omega_K}$:

$$\hat{a}_{\omega_K}|U\rangle = 0 \quad \text{and} \quad \hat{a}^{\mathrm{in},r}_{\omega,I}|U\rangle = 0. \tag{74}$$

The Bogoliubov transformations between two sets of the creation and annihilation operators are expressed as

$$\hat{a}_H^{\text{in},r} = \int d\omega_K [\alpha^r_{\omega_K,\omega}\hat{a}_{\omega_K} + \beta^{r*}_{\omega_K,\omega}\hat{a}^\dagger_{\omega_K}],$$
$$\hat{a}_H^{\text{in},l} = \int d\omega_K [\alpha^l_{\omega_K,\omega}\hat{a}_{\omega_K} + \beta^{l*}_{\omega_K,\omega}\hat{a}^\dagger_{\omega_K}] \tag{75}$$

with the coefficients [36]

$$\alpha^r_{\omega_K,\omega} = \frac{1}{2\pi\kappa}\sqrt{\frac{\omega}{\omega_K}}(-i\omega_K)^{i\omega/\kappa}\Gamma\left(\frac{-i\omega}{\kappa}\right), \tag{76a}$$

$$\beta^r_{\omega_K,\omega} = \frac{1}{2\pi\kappa}\sqrt{\frac{\omega}{\omega_K}}(-i\omega_K)^{-i\omega/\kappa}\Gamma\left(\frac{i\omega}{\kappa}\right), \tag{76b}$$

$$\alpha^l_{\omega_K,\omega} = \frac{1}{2\pi\kappa}\sqrt{\frac{\omega}{\omega_K}}(i\omega_K)^{-i\omega/\kappa}\Gamma\left(\frac{i\omega}{\kappa}\right), \tag{76c}$$

$$\beta^l_{\omega_K,\omega} = \frac{1}{2\pi\kappa}\sqrt{\frac{\omega}{\omega_K}}(i\omega_K)^{i\omega/\kappa}\Gamma\left(\frac{-i\omega}{\kappa}\right). \tag{76d}$$

After introducing the appropriate quantum state, we are ready to compute the particle densities of each mode produced from the Unruh state as well as the mode mixing due to the existence of the negative norm state and their mode correlators.

V. PARTICLE DENSITIES AND MODE CORRELATORS

We first calculate the particle density of the $\varphi^{\text{out},r}_{\omega,u_r}$ mode in the subsonic region, an analog of the Hawking mode using the Bogoliubov transformations (69) and (75), which can be expressed as the thermal spectrum

$$n^{ur} = \langle U|(\hat{a}^{\text{out},r}_{\omega,u_r})^\dagger \hat{a}^{\text{out},r}_{\omega,u_r}|U\rangle = |T^r_H|^2 \frac{1}{e^{\frac{\omega}{T_{\text{hw}}}} - 1} = \frac{\Gamma_\omega}{e^{\frac{\omega}{T_{\text{hw}}}} - 1} \tag{77}$$

with the Hawking temperature $T_{\text{hw}} = \kappa/2\pi$ even for the gapped excitations shown in Fig. 5. The accompanying graybody factor is obtained as

$$\Gamma_\omega = \frac{\sinh\left(\frac{\pi\omega}{\kappa}\right)\sinh\left(\frac{\pi M_r\eta_r\omega}{\kappa}\right)}{\sinh^2\left(\frac{\pi\omega(1+M_r\eta_r)}{2\kappa}\right)}. \tag{78}$$

The produced particles are mainly due to the introducing Unruh state in the past horizon in the r region where the modes can partially transmit to the future null infinity, giving the analog Hawking radiation. The obtained graybody factor above returns to the expression of the gapless case in Ref. [12] in the limits of $\eta_r = 1$ ($\Omega = 0$). For small

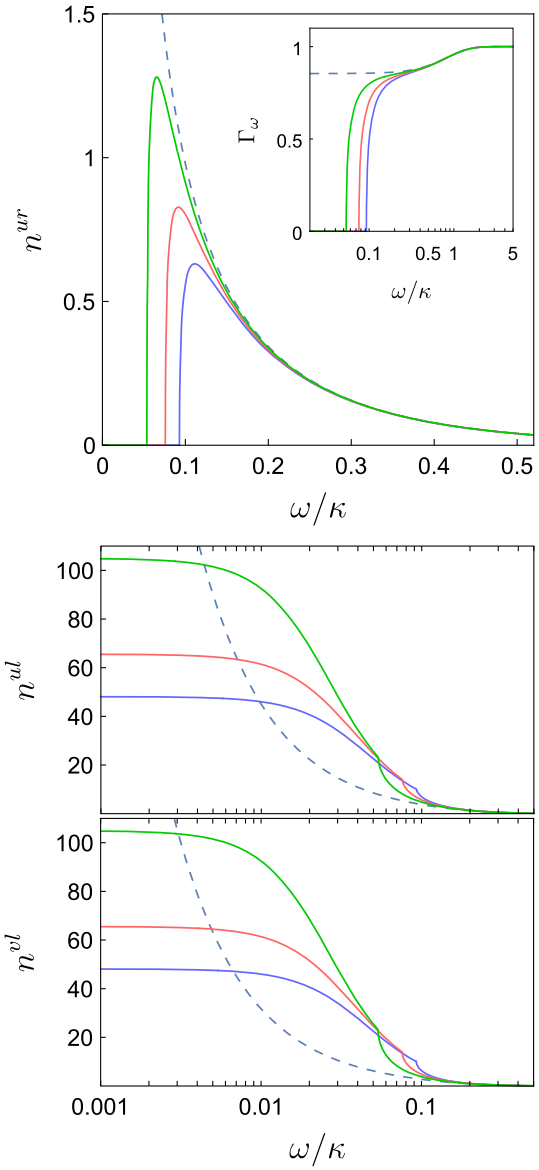

FIG. 5. Plot of the spectrum n^{ur}, n^{ul}, and n^{vl} in (77), (79) and (80) as the function of ω/κ with various values of the Rabi frequency $\Omega/\kappa = 0$ (dashed line), 0.001 (green line), 0.002 (red line), and 0.003 (blue line). Notice that the comparison is made between the gapped cases ($\Omega \neq 0$) and the gapless cases ($\Omega = 0$). The inset in n^{ur} shows the graybody factor Γ_ω in (78). The parameters are the same as those in Fig. 1.

frequency $\omega \ll \kappa$, the graybody factor can be approximated as $4M_r\eta_r/(1 + M_r\eta_r)^2$ which is the same as the graybody factor in the case of the steplike change of the sound speed in Ref. [10] with the constant velocity set to be $v = v_r$ where the dispersive effects can be ignored in such small frequencies. The main influences of the gap energy m_{eff} in (9) to the graybody factor (78) can be seen from the existence of a threshold ω_r where $n^{ur} = 0$ if $\omega < \omega_r$ shown in the inset of Fig. 5. This is just the critical value of frequency, below which in the subsonic region the modes

from the past horizon in the r region will be totally reflected toward the future horizon, giving no Hawking radiation in the future null infinity shown in Fig. 4. This can be realized to rewrite (20) as the time-independent Schrödinger-like equation where ω_a^2 plays a role as the effective potential term. The relative large value of $m_{\rm eff}$ in the subsonic region driven by the large Rabi coupling constant Ω gives the relatively large value of $\omega_{\rm sub}^2$ (22) that leads to the large scattering effects, giving smaller transmission coefficient T_H^r and thus resulting in the smaller graybody factor. When $\omega \to \infty$, $\Gamma_\omega \to 1$ as expected.

Next, we consider particle spectrum of the modes inside the analog horizon, namely $\varphi^{{\rm out},l}_{\omega,v_l}$ and $\varphi^{{\rm out},l}_{\omega,u_l}$. Let us first study the behavior of the $\varphi^{{\rm out},l}_{\omega,u_l}$ mode of the negative norm state, which is also called the partner of the Hawking mode. The particle spectrum is obtained as

$$n^{ul} = \langle U|(\hat{a}^{{\rm out},l}_{\omega,u_l})^\dagger \hat{a}^{{\rm out},l}_{\omega,u_l}|U\rangle = \frac{1}{e^{\frac{\omega}{T_{\rm hw}}}-1}|e^{\frac{\omega}{2T_{\rm hw}}}R_H^l + \mathcal{T}_H^{l*}|^2 + |R_I^l|^2, \tag{79}$$

where the coefficients can be substituted from (51), (57) and (63). Although there is no particle coming from the past null infinity, the nature of the negative norm state of $\varphi^{{\rm out},l}_{\omega,u_l}$ in the supersonic region gives rise to vacuum instabilities due to the mode mixing, triggering particle production due to the contribution of R_I^l. In addition, the scattering of the modes from the Unruh state in the past horizon (in the l and r regions) contributes the particle production due to the coefficients of R_H^l and $\mathcal{T}_H^l$. The net result of the particle spectrum exhibits nonthermal. Figure 5 shows the particle density n^{ul} does not change smoothly across ω_r. The main reason is due to the fact that the modes coming from the past horizon in the r region will totally be reflected to the future horizon when $\omega < \omega_r$, giving the enhancement of the particle production of n^{ul} as compared with the modes with frequencies $\omega > \omega_r$. Also, below threshold frequency ω_r, there does not exist the propagating incoming mode originally from the past null infinity in the subsonic region shown in Fig. 4 (middle), giving the vanishing of R_I^l when $\omega < \omega_r$. It is worth mentioning that in the limit $\omega \to 0$, the particle density has a finite saturated value rather than an infrared divergence for the gapless case [32]. Also, for large frequency $\omega \gg \kappa$, it is expected that the incoming mode from the past null infinity will travel directly through the future horizon and toward the future null infinity. Also, the modes from the Unruh states in the past horizon with such large frequencies will travel to the future null infinity. As such, $e^{\frac{\omega}{2T_{\rm hw}}}R_H^l \to 0$, $R_I^l \to 0$, and $\mathcal{T}_H^l \to 1$ render the expression of n^{ul} having a tail of the exponential decay in frequency.

As compared with the $\varphi^{{\rm out},l}_{\omega,u_l}$ mode, the other particle spectrum of emission inside the analog horizon is $\varphi^{{\rm out},l}_{\omega,v_l}$ of the positive norm state where its particle density will have no contribution from the modes in the subsonic region because of the lack of mode mixing giving $R_I^l = 0$, and it becomes

$$n^{vl} = \langle U|(\hat{a}^{{\rm out},l}_{\omega,v_l})^\dagger \hat{a}^{{\rm out},l}_{\omega,v_l}|U\rangle = \frac{1}{e^{\frac{\omega}{T_{\rm hw}}}-1}|e^{\frac{\omega}{2T_{\rm hw}}}\mathcal{R}_H^{l*} + T_H^l|^2 \tag{80}$$

with the coefficients in (50) and (62) shown in Fig. 5 given respectively by the Unruh state in the past horizon in the l and r regions. The particle densities satisfy $n^{ur} + n^{vl} = n^{ul}$ for $\omega > \omega_r$ and $n^{vl} = n^{ul}$ for $\omega < \omega_r$, which can be verified by using the unitary relation $|R_H^l|^2 - |\mathcal{T}_H^l|^2 + |R_I^l|^2 = -1$ accompanied with (52) and (64). The particle densities of n^{ul} and n^{vl} share the same feature that they do not have a smooth change across ω_r.

Here we come to study the mode correlator such as the correlator of the analog Hawking mode $\varphi^{{\rm out},l}_{\omega,u_r}$ in the subsonic region and its partner $\varphi^{{\rm out},l}_{\omega,u_l}$ in the supersonic region as well as the correlator of the $\varphi^{{\rm out},l}_{\omega,u_l}$ mode and the $\varphi^{{\rm out},l}_{\omega,v_l}$, both of which are in the supersonic regions.

The ul-ur correlator can be computed from

$$\begin{aligned} c_{ur,ul} &= \langle U|^{\rm out}\hat{a}^r_{\omega,u}{}^{\rm out}\hat{a}^l_{\omega,u}|U\rangle \\ &= R_I^{l*}R_I^r + \frac{e^{\frac{\omega}{2T_{\rm hw}}}}{e^{\frac{\omega}{T_{\rm hw}}}-1}\left(T_H^r\mathcal{T}_H^l + T_H^r R_H^{l*}e^{\frac{\omega}{2T_{\rm hw}}}\right), \end{aligned} \tag{81}$$

where the coefficients can be found in (42), (51), (56), (57), (62), and (63). Nevertheless, the ul-vl correlator can be obtained as

$$\begin{aligned} c_{vl,ul} &= \langle U|^{\rm out}\hat{a}^l_{\omega,v}{}^{\rm out}\hat{a}^l_{\omega,u}|U\rangle \\ &= R_I^{l*}T_H^l + \frac{1}{e^{\frac{\omega}{T_{\rm hw}}}-1} \\ &\quad\times\left[R_H^{l*}T_I^l e^{\frac{\omega}{T_{\rm hw}}} + (\mathcal{T}_H^l T_I^l + \mathcal{R}_H^{l*}R_H^{l*})e^{\frac{\omega}{2T_{\rm hw}}} + \mathcal{T}_H^l\mathcal{R}_H^{l*}\right], \end{aligned} \tag{82}$$

where the coefficients can be found in (42), (51), (56)–(58), (62), and (63). Both correlators as a function of frequency are shown in Fig. 6. Because there is no particle production below the threshold frequency ω_r in the $\varphi^{{\rm out},r}_{\omega,u_r}$ mode of the analog Hawking mode, the correlator $c_{ur,ul}$ vanishes although the partner mode of the $\varphi^{{\rm out},l}_{\omega,u_l}$ mode of the negative norm state does have particle production within this frequency range. For $\omega > \omega_r$, the correlator $c_{ur,ul}$ shows a peak around the threshold frequency. As for the correlator of $c_{vl,ul}$, apart from the large correlation in small frequency, there exists also a peak near the threshold frequency. Interestingly, as $\omega > \omega_r$, the magnitude of correlator $|c_{ur,ul}|$ for a gapped mode will be larger than gapless cases, especially around the threshold frequency. The behavior of the mode correlators will contribute to the density-density correlators to be done in our forthcoming work that can be measured experimentally [3,4,37].

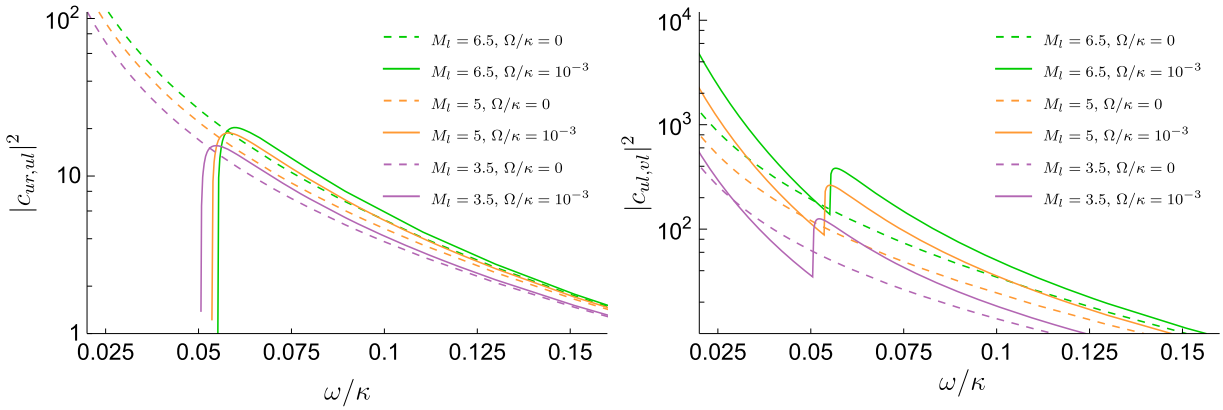

FIG. 6. The magnitude of $|c_{ur,ul}|^2$ and $|c_{ul,vl}|^2$ in (81) and (82) are shown in the left and right panels, respectively. We compare the gapped cases (solid lines) with gapless cases (dashed lines) for various values of Mach number $M_l = 6.5$ (green line), 5 (orange line), and 3.5 (purple line). The other parameters are fixed as $c_l = 0.4$ and $c_r = 1.34$.

VI. SUMMARY AND CONCLUSION

We start from considering the condensates of cold atoms at zero temperature in the tunable binary BEC system with the Rabi transition between atomic hyperfine states where the system can be represented by a coupled two-field model of gapless excitations and gapped excitations. For the general spatial-dependent coupling constant strengths, the decoupling of two excitations under certain conditions of the condensate wave functions and the coupling constants is reviewed. In particular, we will solely focus on the dynamics of gapped excitations. The dispersion relation of the gapped modes involves the k^2 term in a very long wavelength approximation that behaves relativistically. The particular spatial-dependent sound speed and flow velocity with the acoustic horizon in the elongated condensates are introduced so that the equations of the mode functions can be analytically treatable. In addition, the horizon generated from the transonic flow is formed with experimentally accessible parameters. As compared with the gapless excitations, there exists a threshold frequency ω_r in the subsonic region above which the modes can propagate. The asymptotic states of the incoming and outgoing modes are identified where the scattering coefficients between them for various scattering processes can be achieved. Accordingly, the Bogoliubov transformations of the creation and annihilation operators associated with the incoming and outgoing modes are derived. Also, the Unruh state is introduced to be the appropriate state for the description of gravitational collapse of the black hole. The particle spectrum of the analogous Hawking modes in the exterior of the horizon of the subsonic region is computed and is shown as a thermal one with temperature given by the analogous surface gravity κ, mainly due to the introduction of the Unruh state in the past horizon. The associated graybody factor significantly deviates from that of the gapless cases near the threshold frequency, which vanishes as the mode frequency is below ω_r. In the interior region of the horizon of the supersonic region, the spectrum of the particle production of the Hawking partner has the nonthermal feature. The correlators between the Hawking mode and its partner of relevance to the experimental observations show some peaks near the threshold frequency ω_r resulting from the gap energy term. The behavior of the mode correlators will contribute to the density-density correlators that can be measured experimentally to be carried out in our forthcoming work.

ACKNOWLEDGMENTS

This work was supported in part by the Ministry of Science and Technology, Taiwan, Republic of China.

[1] S. W. Hawking, Particle creation by black holes, Commun. Math. Phys. **43**, 199 (1975).
[2] W. G. Unruh, Experimental Black-Hole Evaporation?, Phys. Rev. Lett. **46**, 1351 (1981).
[3] J. R. Muñoz de Nova, K. Golubkov, V. I. Kolobov, and J. Steinhauer, Observation of thermal hawking radiation and its temperature in an analogue black hole, Nature (London) **569**, 688 (2019).
[4] V. I. Kolobov, K. Golubkov, J. R. Muñoz de Nova, and J. Steinhauer, Observation of stationary spontaneous hawking radiation and the time evolution of an analogue black hole, Nat. Phys. **17**, 362 (2021).

[5] J. H. Kim, D. Hong, and Y. Shin, Observation of two sound modes in a binary superfluid gas, Phys. Rev. A **101**, 061601 (2020).
[6] R. Cominotti, A. Berti, A. Farolfi, A. Zenesini, G. Lamporesi, I. Carusotto, A. Recati, and G. Ferrari, Observation of Massless and Massive Collective Excitations with Faraday Patterns in a Two-Component Superfluid, Phys. Rev. Lett. **128**, 210401 (2022).
[7] M. Visser and S. Weinfurtner, Massive Klein-Gordon equation from a bose-einstein-condensation-based analogue spacetime, Phys. Rev. D **72**, 044020 (2005).
[8] U. R. Fischer and R. Schützhold, Quantum simulation of cosmic inflation in two-component Bose-Einstein condensates, Phys. Rev. A **70**, 063615 (2004).
[9] S. Liberati, M. Visser, and S. Weinfurtner, Analogue quantum gravity phenomenology from a two-component Bose–Einstein condensate, Classical Quantum Gravity **23**, 3129 (2006).
[10] W.-C. Syu, D.-S. Lee, and C.-Y. Lin, Analogous Hawking radiation and quantum entanglement in two-component Bose-Einstein condensates: The gapped excitations, Phys. Rev. D **106**, 044016 (2022).
[11] J. Steinhauer, Observation of quantum Hawking radiation and its entanglement in an analogue black hole, Nat. Phys. **12**, 959 (2016).
[12] A. Fabbri, R. Balbinot, and P. R. Anderson, Scattering coefficients and gray-body factor for 1D BEC acoustic black holes: Exact results, Phys. Rev. D **93**, 064046 (2016).
[13] A. Coutant and S. Weinfurtner, Low-frequency analogue Hawking radiation: The Bogoliubov-de Gennes model, Phys. Rev. D **97**, 025006 (2018).
[14] C. J. Myatt, E. A. Burt, R. W. Ghrist, E. A. Cornell, and C. E. Wieman, Production of Two Overlapping Bose-Einstein Condensates by Sympathetic Cooling, Phys. Rev. Lett. **78**, 586 (1997).
[15] D. S. Hall, M. R. Matthews, J. R. Ensher, C. E. Wieman, and E. A. Cornell, Dynamics of Component Separation in a binary Mixture of Bose-Einstein Condensates, Phys. Rev. Lett. **81**, 1539 (1998).
[16] S. B. Papp, J. M. Pino, and C. E. Wieman, Tunable Miscibility in a Dual-Species Bose-Einstein Condensate, Phys. Rev. Lett. **101**, 040402 (2008).
[17] S. Tojo, Y. Taguchi, Y. Masuyama, T. Hayashi, H. Saito, and T. Hirano, Controlling phase separation of binary Bose-Einstein condensates via mixed-spin-channel feshbach resonance, Phys. Rev. A **82**, 033609 (2010).
[18] M. R. Matthews, D. S. Hall, D. S. Jin, J. R. Ensher, C. E. Wieman, E. A. Cornell, F. Dalfovo, C. Minniti, and S. Stringari, Dynamical Response of a Bose-Einstein Condensate to a Discontinuous Change in State, Phys. Rev. Lett. **81**, 243 (1998).
[19] E. Nicklas, H. Strobel, T. Zibold, C. Gross, B. A. Malomed, P. G. Kevrekidis, and M. K. Oberthaler, Rabi Flopping Induces Spatial Demixing Dynamics, Phys. Rev. Lett. **107**, 193001 (2011).
[20] C. Hamner, J. J. Chang, P. Engels, and M. A. Hoefer, Generation of Dark-Bright Soliton Trains in Superfluid-Superfluid Counterflow, Phys. Rev. Lett. **106**, 065302 (2011).
[21] C. Hamner, Y. Zhang, J. J. Chang, C. Zhang, and P. Engels, Phase Winding a Two-Component Bose-Einstein Condensate in an Elongated Trap: Experimental Observation of Moving Magnetic Orders and Dark-Bright Solitons, Phys. Rev. Lett. **111**, 264101 (2013).
[22] W.-C. Syu, D.-S. Lee, and C.-Y. Lin, Analogue stochastic gravity phenomena in two-component Bose-Einstein condensates: Sound cone fluctuations, Phys. Rev. D **99**, 104011 (2019).
[23] R. Balbinot, A. Fabbri, S. Fagnocchi, A. Recati, and I. Carusotto, Nonlocal density correlations as a signature of Hawking radiation from acoustic black holes, Phys. Rev. A **78**, 021603 (2008).
[24] A. Recati, N. Pavloff, and I. Carusotto, Bogoliubov theory of acoustic Hawking radiation in Bose-Einstein condensates, Phys. Rev. A **80**, 043603 (2009).
[25] J. Macher and R. Parentani, Black/white hole radiation from dispersive theories, Phys. Rev. D **79**, 124008 (2009).
[26] P.-E. Larré, A. Recati, I. Carusotto, and N. Pavloff, Quantum fluctuations around black hole horizons in Bose-Einstein condensates, Phys. Rev. A **85**, 013621 (2012).
[27] L. W. Clark, L.-C. Ha, C.-Y. Xu, and C. Chin, Quantum Dynamics with Spatiotemporal Control of Interactions in a Stable Bose-Einstein Condensate, Phys. Rev. Lett. **115**, 155301 (2015).
[28] N. Arunkumar, A. Jagannathan, and J. E. Thomas, Designer Spatial Control of Interactions in Ultracold Gases, Phys. Rev. Lett. **122**, 040405 (2019).
[29] A. Di Carli, G. Henderson, S. Flannigan, C. D. Colquhoun, M. Mitchell, G.-L. Oppo, A. J. Daley, S. Kuhr, and E. Haller, Collisionally Inhomogeneous Bose-Einstein Condensates with a Linear Interaction Gradient, Phys. Rev. Lett. **125**, 183602 (2020).
[30] R. Balbinot, A. Fabbri, R. A. Dudley, and P. R. Anderson, Particle production in the interiors of acoustic black holes, Phys. Rev. D **100**, 105021 (2019).
[31] R. A. Dudley, P. R. Anderson, R. Balbinot, and A. Fabbri, Correlation patterns from massive phonons in $1+1$ dimensional acoustic black holes: A toy model, Phys. Rev. D **98**, 124011 (2018).
[32] A. Coutant, A. Fabbri, R. Parentani, R. Balbinot, and P. R. Anderson, Hawking radiation of massive modes and undulations, Phys. Rev. D **86**, 064022 (2012).
[33] G. Jannes, P. Maïssa, T. G. Philbin, and G. Rousseaux, Hawking radiation and the boomerang behavior of massive modes near a horizon, Phys. Rev. D **83**, 104028 (2011).
[34] F. Michel, J.-F. m. c. Coupechoux, and R. Parentani, Phonon spectrum and correlations in a transonic flow of an atomic bose gas, Phys. Rev. D **94**, 084027 (2016).
[35] R. A. Dudley, A. Fabbri, P. R. Anderson, and R. Balbinot, Correlations between a Hawking particle and its partner in a $1+1$D Bose-Einstein condensate analog black hole, Phys. Rev. D **102**, 105005 (2020).
[36] P. R. Anderson, R. Balbinot, A. Fabbri, and R. Parentani, Hawking radiation correlations in Bose-Einstein condensates using quantum field theory in curved space, Phys. Rev. D **87**, 124018 (2013).
[37] J. Steinhauer, Measuring the entanglement of analogue Hawking radiation by the density-density correlation function, Phys. Rev. D **92**, 024043 (2015).